Determination of oxidation rates and volatile oxidation products for HTGR graphite matrix material exposed to steam atmospheres

Brian A. Brigham [a,†], Katherine I. Montoya [a], Tyler J. Gerczak [b], Elizabeth S. Sooby [a]

[a] Department of Physics and Astronomy, University of Texas at San Antonio, San Antonio, TX 78249, USA
[b] Nuclear Energy and Fuel Cycle Division, Oak Ridge National Laboratory, Oak Ridge, TN 37831, USA

Abstract

High-temperature gas-cooled reactors (HTGRs) in operation use tristructural isotropic (TRISO) particles embedded in graphite and carbonized resin matrix to form the fuel element. This graphite matrix material serves as a supportive structural element, heat transfer medium, and neutron moderator. In HTGR designs, fuel compacts are exposed to helium coolant, which facilitates high outlet temperatures (750°C<T<950°C) and subsequently greater thermal efficiency than current commercial power reactors. However, data pertaining to the oxidation resistance of graphite matrix material in HTGR accident or off-normal conditions (<50k kPa pH_2O, 800°C<T<1600°C) is limited. In this study, both the oxidation behavior of matrix graphite material and its gas-phase products, including CO, CO_2, and H_2, are quantified in varied oxidant atmospheres using a coupled thermogravimetric analyzer and mass spectrometer. Oxidation rates reported here for varied steam (H_2O [g]) atmospheres are predominantly linear and comparable with literature values in the range of tested temperatures (800–1200°C). Changes in dominant matrix oxidation products from primarily CO to a mixture of CO, CO_2, and H_2 were observed at higher temperatures (≥1000°C) and steam atmospheres (≥5 kPa pH_2O). Kinetic data indicates that there was no shift in oxidation regime with chemical oxidation occurring at all temperatures and H_2O (g) atmospheres tested. These data provide insight into the oxidation behavior of graphite matrix material and will inform future testing conditions, notably mixed atmospheric conditions, of HTGR fuel elements.

Highlights

- Oxidation results of matrix material at 800–1200°C under varied H_2O (g) atmospheres
- Temperature is the dominant variable for oxidation rates and volatile gas production in H_2O (g) atmospheres
- Matrix oxidation products shift from predominantly CO to greater relative concentrations of CO_2 to CO at increased testing temperatures and/or steam atmospheres

Keywords

Graphite matrix material, high-temperature oxidation, matrix oxidation products, high-temperature gas-cooled reactors, nuclear materials

[†] Corresponding author: *E-mail address:* brian.brigham@utsa.edu (Brian Brigham)

1. Introduction

High-temperature gas-cooled reactors (HTGRs) use fuel elements composed of tristructural isotropic (TRISO) coated particle fuel consisting of uranium-bearing kernels encapsulated in both carbon and silicon carbide layers smaller than 1 mm in diameter [1]. These particles are shaped into right cylinder compact geometries for prismatic core designs and spherical geometries for pebble bed reactors to form fuel elements consisting of 1,000s of particles, in which graphite matrix material encapsulates TRISO particles, providing structural support and protecting them from damage [2]. During nominal operating conditions, the pebble bed fuel elements are exposed to helium coolant, facilitating high outlet temperatures (750°C<T<950°C) and higher thermal efficiency relative to current commercial light water reactors [3]. The helium coolant, under nominal operating conditions, contains part per million (ppm) levels of oxidants [4]. Certain accident or off-normal scenarios could introduce air and H_2O (g), which in combination with high temperatures (up to 1600°C) would lead to the oxidation of graphite matrix material. Degradation of the graphite matrix material can potentially expose and subsequently compromise the structural integrity of the TRISO fuel particles [2, 5]. The Department of Energy (DOE) Advanced Gas Reactor (AGR) program supports research to investigate the oxidation response of HTGR materials to oxidant ingress [6]. By testing graphite matrix material and the TRISO fuel separately, the oxidation behavior of graphite matrix material can be isolated and quantified to inform qualification efforts as well as develop fuel performance models to advance this fuel form.

Graphite matrix material differs from traditional nuclear-grade graphites because the matrix requires an alternative fabrication process to protect the embedded TRISO particles from damage. Graphite matrix material is formed by blending phenolic resin (binder) with natural and synthetic flakes (filler) followed by drying and milling [7]. The fuel elements are then formed by overcoating, loading them into a die, pressing particles into shape, and carbonization, with a final heat treatment, which also drives out impurities, at a temperature of 1800–2000°C, compared to the 2500–2800°C anneal temperature of nuclear-grade graphite [8]. The lower heat treatment temperature results in a composite material with partial graphitization of the binder, resulting in more disordered structure relative to nuclear-grade graphite [9-13]. Less oxidative testing has been conducted with graphite matrix material relative to the more well-studied nuclear-grade graphite [14]. The majority of existing graphite matrix materials testing efforts have explored the preferential oxidation of the binder relative to graphitic flakes in the composite structure. In air, the binder has been demonstrated to have lower activation energy than graphitic flakes [10, 15, 16]. Consequently, the reaction rate for graphite matrix material has two maxima as a function of percent sample oxidation during a thermal ramp [17]. There has been little high-temperature oxidation research with graphite matrix material in partial pressures of oxidants simulating off-normal HTGR conditions [6], with the majority of testing performed in atmospheric air [16] or low partial pressure H_2O (g) conditions relevant to chronic oxidation [18, 19].

In accident or off-normal conditions, oxidants can be introduced to the core, often accompanied by elevated temperatures [20-22]. O_2 ingress can be caused by a leak or break in the helium pressure boundary, which leads to the displacement of helium coolant by outside air, resulting in high partial pressure O_2 (pO_2) atmospheres (1 kPa≤pO_2≤20 kPa) and temperatures (800°C≤T≤1600°C) [23, 24]. H_2O (g) ingress events can be caused by a breach in the secondary heat transfer loop and/or depressurization of the primary coolant systems [25]. In accident scenarios, temperature ranges between 1000–1630°C and partial pressures of H_2O (pH_2O) up to 400 kPa are possible [20, 21, 26, 27]. While these events are extremely unlikely (10^{-4}–10^{-6} events year^{-1}) [28], the impact of acute corrosion of graphitic materials in the HTGR core and the subsequent exposure of fuel particles to oxidizing conditions warrant further

study. The magnitude of each event is largely dependent on the location of the breach, timescale of the accident, and quantity of oxidant ingress.

Presented here are the oxidation rates and decomposition modes of graphite matrix materials with select partial pressures of H_2O (g) (pH_2O), in combination with elevated temperatures, to establish graphite matrix material oxidation kinetic behavior over a broad range of potential accident conditions. Furthermore, this study quantifies the production of gaseous by-products of graphite matrix material oxidation, including carbon monoxide (CO), carbon dioxide (CO_2), and hydrogen gas (H_2). These gaseous by-products not only complicate graphite matrix material oxidation reactions but also impact the potential oxidation behavior of TRISO particles embedded in the graphite matrix material [29]. Graphite matrix material downstream from H_2O (g) ingress will likely be exposed to a mix of H_2O (g) and oxidation products, as H_2O (g) will react with carbonaceous materials, influencing downstream oxidation. Quantifying CO, CO_2, and H_2 will advance the community's understanding of matrix oxidation behavior and facilitate precision testing of both graphite matrix material and TRISO fuel particles in tightly engineered mixed atmospheres that are representative of these off-normal conditions.

2. Background

Despite the differences between graphite matrix material and nuclear-grade graphite noted above, the existing literature on nuclear-grade graphite provides a useful starting point. Graphite is an excellent neutron moderator and was developed as such in addition to reflector and structural materials for both current and several proposed HTGR reactor designs [30, 31]. Nuclear-grade graphite's oxidation properties have been tested extensively with the majority of research efforts conducted in air. These studies established and corroborated three oxidation regimes, demonstrating Arrhenius temperature dependence for nuclear-grade graphite [6, 23, 32, 33]. In the chemical regime (T≤500°C in air), oxidation behavior of graphite is controlled by the rate of the chemical reaction. Additionally, in the chemical regime, the reaction rate is slow relative to gas mass transport, and hence oxidation occurs uniformly throughout material. At higher temperatures (500°C<T<800°C in air), the reaction rate of graphite oxidation increases and limits the penetration of oxidant throughout the sample. In the pore-diffusion regime, local oxidization creates pores in the sample. At even higher temperatures (T≥800°C in air), in the boundary layer regime, the chemical reactivity increases further, limiting the reaction to the surface and boundary layer of graphite samples. In both of these latter regimes, oxidation is largely controlled by surface oxidant concentrations and the mass transfer of gas species (O_2, CO, CO_2) at the boundary layer [34]. The exact temperatures between regimes vary based upon the material properties, such as filler size, morphology, natural graphitic percentage, and general microstructure among the nuclear grades of graphite [16]. Importantly, the temperature regimes can vary for different partial pressures or types of oxidants. To the authors' understanding, the oxidation testing of nuclear-grade graphite in H_2O (g) atmospheres has been largely limited to conditions designed to simulate normal operating conditions (sub ppm levels of H_2O (g). These tests utilized elevated pH_2O (0.005-0.5 kPa), to ensure oxidation could be measured in reasonable time-scales, and typically tested at temperatures <1000°C which resulted in oxidation kinetics that would fall in the chemical oxidation regime [18, 19]. Under these conditions, oxidation rates were slow corroborating chronic oxidation measured on the timescale of months to years in test HTGR reactors [4].

Oxidation testing of matrix graphite material is sparse relative to nuclear-grade graphite and has largely not be conducted in HTGR accident conditions. Due to varied microstructural properties, the temperature onsets of the pore-diffusion and boundary layer regimes, as well as kinetic parameters of matrix graphite material, are not correlated or relevant to the nuclear-grade graphite sample type [10]. Recent research by Gerczak et al. [6] demonstrated a departure of graphite matrix material from the modeled chemical regime at both high temperatures (1200°C<T<1500°C) and high pH_2O (10 kPa<

pH$_2$O<48 kPa). Further, Montoya et al. [13] has confirmed the assessment of preferential oxidation of the binder over graphitic flakes in 20% H_2O (g) atmosphere using electron microscopy and Raman spectroscopy techniques. The work by Gerczak and Montoya et al. motivates further testing and characterization of the oxidation behavior of graphite matrix material over the full range of oxidizing atmospheres and temperatures anticipated in off-normal accident conditions.

Oxidation of carbon-based materials in H_2O (g) atmospheres is further complicated by the inhibition of the oxidation reaction by a by-product, H_2 [24, 35, 36]. The primary heterogeneous reaction is given by global graphite oxidation in Equation 1:

$$C\ (s)\ + H_2O\ (g) = CO\ (g) + H_2\ , \qquad (1)$$

H_2 and H_2O (g) compete for graphite binding sites, limiting the rate of the reaction. This complicated non-linear reaction can be explained by the Langmuir-Hinshelwood model at low partial pressure of H_2O (g) and other oxidants [19] and within the chemical regime, conditions which are similar to nominal HTGR conditions [4]. However, at higher partial pressures of oxidants and/or temperatures, typical of accident conditions, extrapolation from the LH model is more difficult and requires empirical observations [6, 37].

Further complicating graphite oxidation in H_2O (g) atmospheres are secondary reactions that both produce and consume oxidation by-products given in Equations 2–4 [34, 36]:

$$CO\ (g) + H_2O\ (g) = CO_2\ (g) + H_2\ (g)\ , \qquad (2)$$
$$CO_2\ (g) + C\ (s) = 2CO\ (g)\ , \qquad (3)$$
$$C\ (s) + 2H_2\ (g) = CH_4\ (g)\ , \qquad (4)$$

Equations 1 and 4 occur only at the surface of the graphite sample, while Equations 2 and 3 occur throughout the gas phase of the reaction. Both reactions described in Equations 3 and 4 require high partial pressures of reactants to occur, which are likely not possible in HTGR off-normal conditions [38, 39]. The relative quantities of graphite matrix material oxidation products that will be produced in off-normal HTGR conditions are unknown as reaction rates will be governed by both the evolving microstructure of graphite matrix material as well as varied oxidant concentrations. CO and CO_2 will also impact graphite matrix material downstream in other parts of the HTGR in unknown ways, as they may induce secondary oxidation of pebble fuel elements.

3. Methods

Graphite matrix material samples were fabricated following similar procedures defined by the fabrication effort for the fifth, sixth, and seventh Advanced Gas Reactor Fuel Qualification and Development Program irradiation experiments (AGR-5/6/7) to produce matrix only, or “blank,” samples at Oak Ridge National Laboratory (Oak Ridge, TN, US), as described in detail by Gerczak et al. [6]. Received samples were discs measuring 12 mm in diameter and 2.5 mm thick weighing approximately 500 mg each (geometric density 1.75 +/- 0.05 g cm^{-3}). Samples were composed of natural graphite, synthetic graphite, carbonized resin binder (19%), and hardening agent (1%). Before testing, each sample was cut into ~250 mg semicircular halves and then sonicated in acetone followed by methanol for 20 minutes using a VWR Symphony Sonicator (Radnor, PA, US). After cleaning, the samples were placed in a Thermcraft XSB box furnace (Winston-Salem, NC, US) at temperatures of ~110°C for 1–1.5 hours to drive off excess moisture and cutting solutions prior to testing.

Mass loss and oxidation gas by-products were measured with a paired Netzsch F3 449 Jupiter simultaneous thermal analyzer (STA) and Netzsch 403 D Aëolos quadrupole mass spectrometer (QMS;

Selb, DE). To verify instrument performance and methodology, limited oxidation testing in O_2-containing atmospheres was conducted at the University of Texas at San Antonio with a STA equipped with a silicon carbide furnace and alumina protective tube. Gettered argon (Ar) with <1.0 x 10^{-8} ppm O_2 was used to ensure that samples were exposed to appreciable oxidants only at isothermal testing temperatures. The thermocouple used for testing was calibrated with melt point standards (tin, bismuth, zinc, aluminum, silver, and gold), provided by Netzsch (part number 6.223.5-91.3). Oxidation testing conditions of 0.71 kPa pO_2 at 800°C (n=3) and 19 kPa pO_2 at both 800 and 1200°C are summarized in Table 1. O_2 was added as synthetic air (21% O_2/79% Ar for 19 kPa pO_2) or as 1% O_2 (1% O_2/99% N_2 for 0.71 kPa pO_2) through internal STA mass flow controllers. A 2100 RapidOx (Cambridge Sensotec, St. Ives, UK) paired with O_2 sensors located at the inlet and outlet of the furnace was used to monitor the STA for possible atmospheric contamination prior to and during oxidation testing. The O_2 contaminant level in the systems was demonstrated never to exceed that predicted by the law of mass action [40].

H_2O (g) oxidation tests of graphite matrix material samples were performed at Netzsch Headquarters (Selb, DE) with a combination of three varied oxidizing atmospheres (0.85, 5.0, and 50 kPa pH_2O) and temperatures (800, 1000, and 1200°C) with the same Netzsch model STA used at UTSA paired with a QMS. H_2O (g) was produced by the Netzsch water vapor generator or bubbler, depending on target partial pressure, and introduced to the furnace via a heated (200°C) stainless steel transfer line (Table 2). Additional heaters (set to 200°C) were used at the furnace adapter head and collar to prevent condensation of H_2O (g) prior to injection in the hot zone of the furnace. The Netzsch QMS was used to quantify mass species of 2 (H_2), 4, 18 (H_2O), 28 (CO), 32 (O_2), 40 (Ar), and 44 (CO_2) for the H_2O (g) tests with approximately 30 scans per second. For both O_2 and H_2O (g) testing, graphite matrix material samples were tested on alumina platforms with the oxidant introduced from the top of the furnace, downward onto each sample. Isothermal testing was performed; specifically, samples were exposed to gettered Ar during ramp and allowed to equilibrate for 30 minutes at the final testing temperature before the oxidant was introduced. Samples were exposed to the oxidant for 6 hours [40].

A Hitachi FlexSEM1000 scanning electron microscope (SEM) (Tokyo, JP), equipped with secondary and backscatter electron detectors as well as energy dispersive spectroscopy (Oxford Instruments, Oxford, UK), was used to characterize graphite matrix material samples both pre- and post-oxidation testing. Imaging provided insight into formed microstructures as a result of different oxidant exposures, kinetic regimes, and degradation mechanisms. Micrographs also provided a quantitative method for determining the depth of oxidative attack and assessing if oxidation kinetics were either surface dependent or bulk reactions.

Mass change as well as oxidation rate (i.e., mass loss as a function of time) were normalized to initial exposed surface area for each individual sample. Raw oxidation and mass spectrometry data were exported from Netzsch Proteus software (v. 8.0) into .CSV file format. The first derivative of each mass loss curves was used to determine mass loss rates, which were smoothed in Proteus for presentation. An examination of Ar (mass 40, 36, and 38) and O_2 (mass 32, 33, and 34) isotopes' natural abundance vs. signal intensity (Amperes [A]) demonstrates that this signal is well correlated to relative concentration (Table 3). As such, signal intensity was used to compare the relative concentrations of oxidation species during oxidant exposure. Species analyzed include H_2, CO, CO_2, and CH_4.

4. Results

Temperature was identified as the dominant variable governing graphite matrix materials oxidation rates (Fig. 1, Table 4). Increased testing temperatures increased oxidation rates substantially for all tested steam atmospheres. Under 0.85 kPa pH_2O atmospheres oxidation rates of graphite matrix material were 0.346 and 8.72 mg cm^{-2} hr^{-1} at 1000 and 1200°C, respectively (25× increase) under 5.0 kPa pH_2O atmospheres oxidation rates were 0.0534, 2.5, and 22.3 mg cm^{-2} hr^{-1} at 800, 1000, and 1200°C (25

and 9× increases), respectively, and under 50 kPa pH_2O atmospheres oxidation rates were 0.134, 6.92, and 79.9 mg cm^{-2} hr^{-1} at 800, 1000, and 1200°C, respectively (52 and 12× increases). Oxidation rates were largely linear throughout the isotherm for all testing conditions, except for 50 kPa pH_2O at 1200°C (Fig. 1b), in which the sample was consumed and saw varied oxidation rates as the exposed surface area became large and irregular compared with the initial state of the sample. Water mass signal was consistent for each testing condition demonstrating consistent supply of oxidant throughout each run (Fig. 2). Increased graphite matrix oxidation was observed at all testing temperatures as pH_2O was increased from both 0.85–5.0 kPa pH_2O and 5.0-50 kPa pH_2O. However, these differences were not as significant as those observed in graphite matrix material oxidation rates between elevated temperatures for the same pH_2O atmosphere.

Production of CO, CO_2, and H_2 was greatest at higher temperature and H_2O (g) atmospheres (Fig. 3). For all test conditions, barring the 50 kPa pH_2O at 1200°C testing condition, CO mass signal was far greater than both H_2 and CO_2 signals (Table 5). As was the case for oxidation rates, enhanced temperatures (from 800 to 1000°C or 1000 to 1200°C) increased volatile gas product signal. For example, under 0.85 kPa pH_2O, CO signal was 1.41×10^{-10} and 2.52×10^{-10} A at 1000 and 1200°C, respectively (1.8× increase). Under 5.0 kPa pH_2O, CO signal was 8.16×10^{-11}, 1.07×10^{-10}, and 2.40×10^{-10} A at 800, 1000, and 1200°C, respectively (1.3 and 2.2× increases). Under 50 kPa pH_2O atmospheres, CO signal was 8.93×10^{-11}, 2.40×10^{-10}, and 6.26×10^{-10} A at 800, 1000, and 1200°C, respectively (2.7 and 2.6× increases). Enhanced production of H_2 and CO_2 under enhanced temperatures and pH_2O atmospheres followed the same trends (Table 5). For all conditions, barring the 50 kPa pH_2O at 1200°C, where the sample was consumed, volatile gas product signal was consistent (Fig. 4). Using quadrupole mass spectrometry, the CH_4 signal was confounded by O signal, which was produced from the dissociation of H_2O during the oxidant isotherm. However, when the data was normalized to account for the confounding signal, no significant CH_4 production was observed. Further, the CH_4 signal was similar between the 800, 1000, and 1200°C testing conditions for each H_2O (g) atmosphere, indicating no production (data not shown).

Increased CO, H_2, and CO_2 mass signal was observed in increasing H_2O (g) atmospheres and/or temperature testing conditions. However, increased signal was not uniform for all three species as shown in a plot of the ratios of average isotherm mass signal intensity (Fig. 5). Mass signal increased with elevated temperature and pH_2O atmospheres for all mass species, however, the increase in the H_2 and CO_2 mass signal was greater than the increase in CO mass signal relative to the low temperature (e.g. 800°C) and pH_2O (e.g. 0.85 and 5.0 kPa pH_2O) atmosphere testing conditions. This is reflected by $CO:H_2$ and $CO:CO_2$ ratios <1 at the most extreme testing conditions of 1200°C and 50.0 kPa pH_2O, the only testing condition in which average H_2 and CO_2 signals were greater than CO signal. All other testing conditions had greater CO mass signals relative to both H_2 and CO_2 resulting in $CO:H_2$ and $CO:CO_2$ ratios >1. $CO:H_2$ ratios were dictated largely by H_2O (g) atmospheres, with 5.0 kPa, and 50 kPa pH_2O conditions producing $CO:H_2$ ratios of 15.9, 3.54, and 1.56, respectively at 1000°C, and 12.2, 1.85, and 0.88, respectively at 1200°C. Conversely, $CO:CO_2$ ratios were dictated largely by temperature, with 1000, and 1200°C testing conditions producing $CO:CO_2$ ratios of 24.0, 14.7, and 2.71, respectively under 5.0 kPa pH_2O atmospheres and 18.1, 3.35, and 0.84, respectively under 50 kPa pH_2O atmospheres. The 800°C at 0.85 kPa pH_2O testing condition was not included for analysis due to a high H_2O and O_2 mass spectrometry signal observed throughout the run, including the inert ramp, indicating that an oxidant level above the intended partial pressure was introduced to the sample. The ratios of $CO:CO_2$ and $CO:H_2$ is a potentially important indicator of oxidation behavior, indicative of the thermochemical state of

matrix graphite as oxidation occurs.

5. Discussion

5.1. O_2 atmosphere test results and comparison to relevant literature

Graphite matrix material oxidation behavior under O_2 atmospheres performed as expected, largely corroborating literature results, and helping to further validate the methodology used here. Overall, there was rapid oxidation observed in 19 kPa pO_2 atmosphere at both 800 and 1200°C, with oxidation rates of 119 and 361 mg cm^{-2} hr^{-1}, respectively (Table 6, Fig. 6). The oxidation rate was reproducible for the low O_2 atmospheres condition (0.71 kPa pO_2), which was repeated three times. Here, the oxidation rates of samples are expressed as mg cm^{-2} min^{-1}, with the surface area normalization calculated for the as-received sample specimen, as graphite oxidation rates are largely dependent on sample geometries and size [32]. Oxidation rates are also presented as sec^{-1} for comparison with other studies that normalized rates to initial sample mass. The as-received graphite samples displayed low porosity and a relatively uniform microstructure (Fig. 7a). Post-oxidation, the formation of voids due to material depletion was observed. Specifically, the samples underwent binder evolution, increasing the exposed surface area of the sample at 800°C (Fig. 7b). The sample exposed to the 800°C (Fig. 7c) testing condition had similar evolved microstructure to that seen in Lee et al. where binder evolution caused the flake separation.

Graphite matrix material oxidation data available in the literature are sparse, and studies have varied experimental conditions including sample size, sample grade, flow conditions, and testing temperatures amongst other differences making rate comparisons difficult [40]. For example, Lee et al. [11] demonstrated oxidation rates 15× slower than demonstrated here in air atmospheres likely due to varied sample grade (GKrS [16% resin] vs. ARB 5/6/7 [19% resin] used here) and lower temperatures (750°C vs. 800°C used here) (Table 7). Additional comparisons of matrix graphite material oxidation rates with nuclear grade graphite are difficult due to the more reactive nature of matrix graphite material [11]. The oxidation rate of 119 mg cm^{-2} hr^{-1} of graphite matrix material tested here at 800°C was 3× greater than- and similar to oxidation rates for nuclear grade graphite determined by Fuller and Okoh [30] and Chi and Kim [41], respectively. In the next sections, we compare graphite matrix material oxidation rate data under steam atmospheres. The most extensive oxidation testing study done to date, by Gerczak et al. [6], used similar experimental conditions to those utilized here. This, and the present study yielded oxidation rates that were highly comparable, with only 6% difference between studies.

5.2. Oxidation behavior in H_2O (g) atmospheres

The driving variable for graphite matrix material oxidation rates was temperature under the range of H_2O (g) atmospheres (0.85–50 kPa pH_2O) tested here. The oxidation rate of graphite matrix material averaged across all H_2O (g) atmospheres at 1200°C was 800× and 15× greater than the 800 and 1000°C testing conditions, respectively, while increased H_2O (g) atmospheres at the same temperature increased oxidation rates less than an order of magnitude as measured by Δmass, shown in Fig. 1. The greater impact of increased temperature vs. increased H_2O (g) partial pressures is predicted by Equations 1 and 2 with nuclear-grade graphite [39], which is corroborated in this study with graphite matrix material. Significant increases in oxidation rate as a function of temperature were observed between the 800 and 1200°C testing conditions. However, an Arrhenius plot of the average six hour log reaction rate plotted against inverse temperature for each H_2O (g) atmosphere did not indicate a shift an oxidation regime (Fig. 8) [14, 30]. Nor was any shift in oxidation regime observed when isolated one-hour segments of the isotherm, including the hour of greatest oxidation, were used to create the plot

(data not shown). When nuclear grade graphite oxidation rates in O_2 atmospheres are compared between published studies, lower flow rates result in higher transition temperatures between oxidation regimes and lower oxidation rates [16]. However, the flow rate in this study (Table 2) was sufficient and it can be concluded that the tests performed here were oxidant saturated as made clear by both the consistent H_2O (g) mass signal observed throughout the six-hour isotherm for all testing conditions (Fig. 2) and comparable oxidations rate to Gerczak et al. [6] discussed in the next paragraph.

The temperatures that have been used to loosely define the transitions from the chemical regime, pore-diffusion regime, and boundary layer regime were determined empirically in O_2 atmospheres with nuclear-grade graphite [42, 43]. Given the different oxidation kinetics of graphite in H_2O (g) atmospheres [35, 44], it is evident that the transition temperature of graphite matrix material tested here for the chemical to pore-diffusion regime is ≥1200°C, the highest temperature tested here. Accelerated oxidation in H_2O (g) atmospheres is potentially equivalent to the rate of diffusion at these temperatures, resulting in oxidation behavior described in the chemical regime. Lastly, the composite nature of graphite matrix material results in preferential oxidation of binder over graphitic flakes in H_2O (g) atmospheres [6]. It is possible, however, that each of these components is undergoing an oxidation reaction in different regimes simultaneously, possibly confounding interpretation of Arrhenius data.

To date, graphite matrix oxidation and/or nuclear-grade graphite oxidation research has been largely conducted in accelerated tests with H_2O (g) atmospheres (0.005 – 500 kPa pH_2O) designed to simulate atmospheres (<2 ppm) typical of nominal HTGR operating conditions under operational time frames. Early nuclear-grade graphite studies determined that negligible graphite oxidation will occur with H_2O (g) atmospheres ≤0.1 ppm (0.01 Pa) with relatively low oxidation with H_2O (g) atmospheres ≤100 ppm (10 Pa) at temperatures ≤550°C [18, 45]. Approximately 36 years later, Contescu et al. conducted a series of studies that determined the oxidation behavior of multiple nuclear-grade graphite types at a range of H_2O (g) atmospheres (0.010–0.850 kPa pH_2O) and temperatures (800–1100°C) at the lower temperature range of HTGR accident conditions. With nuclear-grade graphite 2114, the average oxidation rate at a range of H_2O (g) atmospheres (0.82–0.97 kPa pH_2O) was 0.12 mg cm^{-2} hr^{-1} at 1000°C [46], 2.9× lower than the graphite matrix material oxidation rate determined in this study (under 0.85 kPa pH_2O). Greater oxidation observed here is due to the composite nature of matrix graphite material relative to nuclear-grade graphite. Preferential oxidation of the binder leads to increased porosity and exposed surface area at lower temperatures, enhancing overall reaction rates relative to nuclear-grade graphite [11]. Rates between Contescu et al. [46] and the study detailed here, however, are difficult to compare given different sample morphologies and instrument setup as discussed previously. Gerczak et al. [6] conducted the most extensive study of graphite matrix material in H_2O (g) atmospheres to date under similar H_2O (g) atmospheres (10–48 kPa pH_2O) and utilized the same sample grade of graphite matrix material (ARB 5/6/7). In addition, the samples used by Gerczak et al. [6] were uncut (~2X diameter) and hung as opposed to placed on a platform like the samples used in this study. Despite these experimental differences, for the one similar testing condition between Gerczak et al. [6] and our study, at 1200°C under ~50 kPa pH_2O, oxidation rates were comparable with values of 1.30 x 10^{-4} sec^{-1} and 1.38 x 10^{-4} sec^{-1} (per initial mass), respectively—both supporting the validity of our testing methodology and data analysis.

5.3. Matrix oxidation products in H_2O (g) atmospheres

The thermodynamics of graphite oxidation in H_2O (g) at temperatures tested here (800– 1200°C) predict that the production of CO and H_2 will be the predominant by-products of graphite oxidation. The primary oxidation pathway is given by the reaction demonstrated in Equation 1 [35]. Overall, CO signal intensity and therefore production was 10× greater than CO_2 signal intensity. Both $CO:H_2$ and $CO:CO_2$ ratios decreased with both increasing H_2O (g) atmospheres and temperatures, indicating that increased

reactant concentrations and temperatures simultaneously increased the global graphite oxidation rate given by Equation 1 and the subsequent reaction of CO and H_2O (g) to form CO_2 and H_2 given by Equation 2. Under 50 kPa pH_2O atmospheres at 1200°C, enhancement of these reactions was evident with $CO:H_2$ and $CO:CO_2$ ratios <1 and noticeable gettering of the testing H_2O (g) atmosphere (Fig. 2). At a constant temperature, oxidation rates increased under greater H_2O (g) atmospheres with apparent saturation occurring between 5 and 50 kPa pH_2O (Fig. 9), potentially similar to the saturation value of 30 kPa pH_2O determined by Gerczak et al. [6]. Overall, CO signal was greater than both H_2 and CO_2 signal for all testing conditions except under 50 kPa pH_2O atmospheres at 1200°C. Conversely, negligible CO_2 production was observed at the 800 and 1000°C testing conditions with significant product observed primarily at 1200°C.

These results demonstrate that at 1200°C, the secondary reaction detailed in Equation 2 was occurring at a greater rate than at the other testing temperatures. There are multiple explanations for these trends. H_2 gas, a by-product of graphite oxidation in H_2O (g), also binds to the graphite surface, inhibiting the oxidation rate of graphite and in turn, inhibiting CO production [19, 36, 37]. Furthermore, over the range of H_2O (g) atmospheres and temperature conditions tested here (5.0 kPa pH_20 at 800°C to 50 kPa pH_20 at 1200°C), increases in both temperature and H_2O (g) enhanced the reaction rate of CO oxidation throughout the gas phase given in Equation 2. This will increase CO_2 and H_2 production and will further inhibit CO production via H_2 inhibition as described previously [39]. When oxidation rates and products at 1200°C were observed simultaneously it was evident that the production of CO, CO_2, and H_2 was greatest in the 50 kPa pH_2O atmosphere testing condition. This indicates far greater oxidation than other testing conditions as CO is consumed to produce CO_2, given by Equation 2, which was balanced by greater production of the CO. The sample tested in this condition was ultimately consumed, and varied oxidation rates were observed over the isotherm (Fig. 1b.).

Additional reactions that would consume H_2 and CO_2 (detailed in Equations 3 and 4) occur primarily at partial pressures (1+ atm) that were not tested. The balance between CO, H_2, and CO_2 graphite matrix material oxidation products is largely the difference in the rate of reactions between Equations 1 and 2 at varied testing conditions. Currently, there are no mass spectrometry data from H_2O (g) oxidation experiments in the literature for $CO:CO_2$ and $CO:H_2$ comparisons. Because the oxidation rates of graphite matrix material at the 50 kPa pH_20 at 1200°C testing condition matches the oxidation rate observed by Gerczak et al. [6], the change in dominant oxidation products observed is likely correlated to the changes in reaction kinetics quantified in that study.

6. Conclusion

Graphite matrix material oxidation rates in O_2 atmospheres were reproducible, similar to literature results, and highlight that varied experiential design parameters, e.g. sample geometry, composition, and thermal history, have significant impact on oxidation behavior. [11]. In H_2O (g) atmospheres, temperature is the dominant variable for both oxidation rates and the production of CO andCO_2. At all pH_2O atmospheres,1200°C testing temperature resulted in significant volatilization of matrix material which did not occur at either 800 or 1000°C. These patterns are predicted by graphite reaction rate calculations in the literature [39] but have not been demonstrated with matrix graphite material. The testing conditions presented here cover a significant portion of temperature and H_2O (g) atmospheres possible under HTGR accident conditions. In combination with Gerczak et al. [6], a broad range of full temperature and H_2O (g) concentrations of accident conditions are tested. Overall, these data in combination with Montoya et al. [13] demonstrate that both temperature and sample morphology are the dominant variables governing oxidation rates in off-normal conditions for proposed HTGR reactions. These data will inform future testing and modeling of accident scenarios, including the impact matrix graphite material oxidation products will have on the HTGR fuel compact. Further mass spectrometry

data from these tests will elucidate the graphite oxidation and gas-phase heterogeneous reactions that occur in HTGR accident conditions.

7. Author credits

Brian A. Brigham: investigation, methodology, writing original draft, writing review, and editing; **Katherine I. Montoya**: microscopy investigation and methodology, writing original draft, writing review, and editing; **Tyler J. Gerczak**: methodology, writing review, and editing; **Elizabeth S. Sooby**: conceptualization, funding acquisition, supervision, writing review, and editing.

8. Acknowledgments

Firstly, we thank the anonymous reviewers whose suggestions greatly improved the quality of the manuscript. We thank Dr. Ekkehard Post from Netzsch Inc. for H_2O (g) atmosphere methodological support and testing. We also thank Mr. Cole Moczygemba for plotting final figure forms. The tested materials were based upon work supported by the US Department of Energy, Office of Nuclear Energy Advanced Gas Reactor Fuel Qualification and Development Program and Department of Energy Nuclear Energy University Programs, Award Number: DE-NE0008798. This report was prepared as an account of work sponsored by an agency of the United States Government. Neither the United States Government nor any agency thereof, nor any of their employees, makes any warranty, express or implied, or assumes any legal liability or responsibility for the accuracy, completeness, or usefulness of any information, apparatus, product, or process disclosed or represents that its use would not infringe privately owned rights. Reference herein to any specific commercial product, process, or service by trade name, trademark, manufacturer, or otherwise does not necessarily constitute or imply its endorsement, recommendation, or favoring by the United States Government or any agency thereof. The views and opinions of authors expressed herein do not necessarily state or reflect those of the United States Government or any agency thereof.

9. References

[1] T. Hicks, Modular HTGR Safety Basis and Approach, INL/EXT--11-22708, Idaho National Laboratory (INL), Idaho Falls, ID (United States), United States, 2011.
[2] P.A. Demkowicz, B. Liu, J.D. Hunn, Coated particle fuel: Historical perspectives and current progress, Journal of Nuclear Materials 515 (2019) 434-450.
[3] A.C. Kadak, The Status of the US High-Temperature Gas Reactors, Engineering 2(1) (2016) 119-123.
[4] X. Yu, S. Yu, Analysis of fuel element matrix graphite corrosion in HTR-PM for normal operating conditions, Nuclear Engineering and Design 240(4) (2010) 738-743.
[5] M. Englert, F. Frieß, M.V. Ramana, Accident Scenarios Involving Pebble Bed High Temperature Reactors, Science & Global Security 25(1) (2017) 42-55.
[6] T.J. Gerczak, C.I. Contescu, Y. Lee, R.W. Mee, A. Schumacher, J. Stempien, M. Trammell, Oxidation of Matrix Material in Helium with Varied Moisture Content, ORNL/TM-2019/1341, Oak Ridge National Lab. (ORNL), Oak Ridge, TN (United States), 2019.
[7] J.D. Hunn, M.P. Trammell, and F.C. Montgomery, Data Compilation for AGR-3/4 Matrix Ring Blank Lot ARB-B1, ORNL/TM-2011/272, Oak Ridge National Lab. (ORNL), Oak Ridge, TN (United States), 2011.
[8] P.J. Pappano, T.D. Burchell, J.D. Hunn, M.P. Trammell, A novel approach to fabricating fuel compacts for the next generation nuclear plant (NGNP), Journal of Nuclear Materials 381(1) (2008) 25-38.

[9] P.P. Magampa, N. Manyala, W.W. Focke, Properties of graphite composites based on natural and synthetic graphite powders and a phenolic novolac binder, Journal of Nuclear Materials 436(1) (2013) 76-83.
[10] R. Moormann, H.K. Hinssen, K. Kuhn, Oxidation Behaviour of an HTR fuel element matrix graphite in oxygen compared to a standard nuclear graphite, Nuclear Engineering and Design 227 (2004) 281-284.
[11] J.J. Lee, T.K. Ghosh, S.K. Loyalka, Oxidation rate of graphitic matrix material in the kinetic regime for VHTR air ingress accident scenarios, Journal of Nuclear Materials 451(1) (2014) 48-54.
[12] W. Windes, T. Burchell, M. Carroll, Graphite Technology Development Plan, INL/EXT-07-13165, Idaho National Laboratory (INL), Idaho Falls, ID (United States), 2010.
[13] K.I. Montoya, C.J. Moczygemba, B.A. Brigham, T.L. Spano, A.A. Campbell, T.J. Gerczak, E.S. Sooby, Determination of preferential binder oxidation in HTGR matrix material subjected to high temperature steam, accepted, Journal of Nuclear Materials (2020).
[14] X. Zhou, C.I. Contescu, X. Zhao, Z. Lu, J. Zhang, Y. Katoh, Y. Wang, B. Liu, Y. Tang, C. Tang, Oxidation Behavior of Matrix Graphite and Its Effect on Compressive Strength, Science and Technology of Nuclear Installations 2017 (2017) 6.
[15] J.J. Lee, T.K. Ghosh, S.K. Loyalka, Oxidation rate of nuclear-grade graphite IG-110 in the kinetic regime for VHTR air ingress accident scenarios, Journal of Nuclear Materials 446(1-3) (2014) 38-48.
[16] C.I. Contescu, S. Azad, D. Miller, M.J. Lance, F.S. Baker, T.D. Burchell, Practical aspects for characterizing air oxidation of graphite, Journal of Nuclear Materials 381(1) (2008) 15-24.
[17] H.-K. Hinssen, K. Kühn, R. Moormann, B. Schlögl, M. Fechter, M. Mitchell, Oxidation experiments and theoretical examinations on graphite materials relevant for the PBMR, Nuclear Engineering and Design 238(11) (2008) 3018-3025.
[18] C. Velasquez, G. Hightower, R. Burnette, Oxidation of H-451 graphite by steam Part I Reaction kinetics, United States, 1978, p. 59.
[19] C.I. Contescu, R.W. Mee, P. Wang, A.V. Romanova, T.D. Burchell, Oxidation of PCEA nuclear graphite by low water concentrations in helium, Journal of Nuclear Materials 453(1) (2014) 225-232.
[20] G.H. Lohnert, The consequences of water ingress into the primary circuit of an HTR-Module - From design basis accident to hypothetical postulates, Nuclear Engineering and Design 134(2) (1992) 159-176.
[21] Y. Zheng, L. Shi, Y. Wang, Water-ingress analysis for the 200MWe pebble-bed modular high temperature gas-cooled reactor, Nuclear Engineering and Design 240(10) (2010) 3095-3107.
[22] R. Moormann, Phenomenology of graphite burning in massive air ingress accidents, 3rd International Topical Meeting on High Temperature Reactor Technology, Johannesburg, South Africa, 2006.
[23] J. Kane, C.I. Contescu, R.E. Smith, G. Strydom, W.E. Windes, Understanding the reaction of nuclear graphite with molecular oxygen: kinetics, transport, and structural evolution, Journal of Nuclear Materials 493 (2017) 343-367.
[24] W. Windes, G. Strydom, J. Kane, R. Smith, Role of nuclear grade graphite in controlling oxidation in modular HTGRs, INL/EXT-14-31720, Idaho National Laboratory (INL), Idaho Falls, ID (United States), 2014.
[25] Preliminary Safety Information Document for the Standard MHTGR. Volume 1, DOE/HTGR-86-024, Stone and Webster Engineering Corp., Boston, MA (United States); Gas-Cooled Reactor Associates, La Jolla, CA (United States), 1986.
[26] N. Iniotakis, C.B. von der Decken, Radiological consequences of a depressurization accident combined with water ingress in an HTR module-200, Nuclear Engineering and Design 109(1) (1988) 299-305.
[27] J. Wolters, R. Bongartz, W. Jahn, R. Moormann, The significance of water ingress accidents in small HTRs, Nuclear Engineering and Design 109(1) (1988) 289-294.

[28] S.J. Ball, Overview Of Modular HTGR Safety Characterization and Postulated Accident Behavior Licensing Strategy, ORNL/TM-2011/187, Oak Ridge National Lab. (ORNL), Oak Ridge, TN (United States), 2014.
[29] E.J. Opila, R.E. Hann Jr., Paralinear Oxidation of CVD SiC in Water Vapor, Journal of the American Ceramic Society 80(1) (1997) 197-205.
[30] E.L. Fuller, J.M. Okoh, Kinetics and mechanisms of the reaction of air with nuclear grade graphites: IG-110, Journal of Nuclear Materials 240 (1997) 241-250.
[31] G. Haag, D. Mindermann, G. Wilhelmi, H. Persicke, W. Ulsamer, Development of reactor graphite, Journal of Nuclear Materials 171(1) (1990) 41-48.
[32] L. Xiaowei, R. Jean-Charles, Y. Suyuan, Effect of temperature on graphite oxidation behavior, Nuclear Engineering and Design 227(3) (2004) 273-280.
[33] E.S. Kim, H.C. No, Experimental study on the oxidation of nuclear graphite and development of an oxidation model, Journal of Nuclear Materials 349(1) (2006) 182-194.
[34] S.H. Chi, C.I. Contescu, T.D. Burchell, Density change of an oxidized nuclear graphite by acoustic mcroscopy and image processing, Journal of Engineering for Gas Turbines & Power, 2009, pp. 1-4.
[35] P.L. Walker, F. Rusinko, L.G. Austin, Gas Reactions of Carbon, in: D.D. Eley, P.W. Selwood, P.B. Weisz (Eds.), Advances in Catalysis, Academic Press1959, pp. 133-221.
[36] R.C. Giberson, J.P. Walker, Reaction of nuclear graphite with water vapor part I. Effect of hydrogen and water vapor partial pressures, Carbon 3(4) (1966) 521-525.
[37] C.I. Contescu, R.W. Mee, Y. Lee, J.D. Arregui-Mena, N.C. Gallego, T.D. Burchell, J.J. Kane, W.E. Windes, Beyond the classical kinetic model for chronic graphite oxidation by moisture in high temperature gas-cooled reactors, Carbon 127 (2018) 158-169.
[38] R. Moormann, Effect of Delays in Afterheat Removal on Consequences of Massive Air Ingress Accidents in High-Temperature Gas Cooled Reactors, Journal of Nuclear Science and Technology 21(11) (1984) 824-835.
[39] W.M. Graven, F.J. Long, Kinetics and Mechanisms of the Two Opposing Reactions of the Equilibrium CO + H2O = CO2 + H21, Journal of the American Chemical Society 76(10) (1954) 2602-2607.
[40] E. Sooby Wood, K.A. Terrani, A.T. Nelson, Sensitivity of measured steam oxidation kinetics to atmospheric control and impurities, Journal of Nuclear Materials 477 (2016) 228-233.
[41] S.-H. Chi, G.-C. Kim, Comparison of the oxidation rate and degree of graphitization of selected IG and NBG nuclear graphite grades, Journal of Nuclear Materials 381(1) (2008) 9-14.
[42] X. Luo, J.-C. Robin, S. Yu, Comparison of Oxidation Behaviors of Different Grades of Nuclear Graphite, Nuclear Science and Engineering 151(1) (2005) 121-127.
[43] M.H. O'Brien, B.J. Merrill, S.N. Ugaki, Combustion testing and thermal modeling of proposed CIT (Compact Ignition Tokamak) graphite tile materials, EGG-FSP-8255, EG and G Idaho, Inc., Idaho Falls, ID (United States), 1988.
[44] E. Sooby Wood, J. Vandegrift, B. Jaques, 4.15 - Steam Oxidation in Accident Conditions, in: R.J.M. Konings, R.E. Stoller (Eds.), Comprehensive Nuclear Materials (Second Edition), Elsevier, Oxford, 2020, pp. 452-473.
[45] M.B. Richards, Reaction of nuclear-grade graphite with low concentrations of steam in the helium coolant of an MHTGR, Energy 15(9) (1990) 729-739.
[46] C.I. Contescu, Y. Lee, R.W. Mee, Oxidation Kinetics by Water Vapor of Nuclear Graphite Grade 2114, ORNL/TM-2018/1057, Oak Ridge National Laboratory, Oak Ridge, TN (United States), 2018.

554 10. Tables

555

556 **Table 1. O_2 testing conditions summary**

Temp. (°C)	Oxidant Conc. (kPa)	Flow rate[a] Ar (sscm)	Flow rate[a] O_2 (sscm)
788	0.71	20	50
	0.71	20	50
	0.71	20	50
800	19	20	200
1200	19	20	200

557

Table 2. H_2O (g) testing conditions summary

Temp. (°C)	Oxidant Conc. (kPa)	Flow rate[a] Ar (sccm)	Evaporation Rate (g hr^{-1})
800	5.0	220	0.5
	50	72	2.5
1000	0.85	20	bubbler
	5.0	220	0.5
	50	72	2.5
1200	0.85	20	bubbler
	5.0	220	0.5
	50	72	2.5

[a]Transfer line (TL) flow rate not listed as differences in flow rate do not greatly impact H_2O (g) atmospheres

561 **Table 3. Isotope natural abundance versus QMS signal**

Elemental Species	Isotope Mass (Da)	Natural abundance (%)	Average signal (A)	Signal (%)
Ar	40	99.6	2.78×10^{-7}	99.5
	36	0.330	1.07×10^{-9}	0.382
	38	0.060	1.98×10^{-10}	0.071
O_2	32	99.5	4.47×10^{-8}	99.5
	34	0.400	1.82×10^{-10}	0.405
	33	0.080	3.59×10^{-11}	0.080

562

563 **Table 4. Summary of Δ mass rate**

Temperature (°C)	Oxidant concentration (kPa)	Isotherm length (min)	Δ mass rate (mg cm^{-2} hr^{-1})	Δ mass rate (sec^{-1})
800	5.0	360	0.0546	9.59×10^{-8}
	50	360	0.134	2.43×10^{-7}
1000	0.85	360	0.346	5.92×10^{-7}
	5.0	360	2.60	4.48×10^{-6}
	50	360	6.92	1.27×10^{-5}
1200	0.85	360	8.72	1.60×10^{-5}
	5.0	360	22.3	4.01×10^{-5}
	50	[a]90	79.9	1.39×10^{-4}

564 [a]Sample was completely consumed, data utilized from first 90 minutes of isotherm

565 **Table 5. Signal intensity for oxidation products[a]**

Temp. (°C)	H_2O (g) conc. (kPa)	Mass species (A)			Ratio	
		CO	H_2	CO_2	CO: H_2	CO: CO_2
800	5.0	8.16×10^{-11}	1.90×10^{-11}	3.41×10^{-12}	4.33	24.0
	50	8.93×10^{-11}	5.40×10^{-11}	4.94×10^{-11}	1.66	18.1
1000	0.85	1.41×10^{-10}	8.85×10^{-12}	1.82×10^{-11}	15.9	7.75
	5.0	1.07×10^{-10}	3.03×10^{-11}	7.30×10^{-12}	3.54	14.7
	50	1.45×10^{-10}	9.69×10^{-11}	4.34×10^{-11}	1.56	3.35
1200	0.85	2.52×10^{-10}	2.08×10^{-11}	3.06×10^{-11}	12.2	8.27
	5.0	2.40×10^{-10}	1.30×10^{-10}	8.87×10^{-11}	1.85	2.71
	50	6.26×10^{-10}	7.08×10^{-10}	7.44×10^{-10}	0.88	0.84

566 [a]Listed values are averages of all data within isotherm

567 **Table 6. Summary of Δ mass rate for O_2 atmospheres**

Temperature (°C)	Oxidant concentration (kPa)	Isotherm length (min)	Δ mass rate (mg cm^{-2} hr^{-1})	Δ mass rate (sec^{-1})
788	0.71	60	1.80	3.13×10^{-6}
	0.71	60	1.71	3.25×10^{-6}
	0.71	60	1.58	3.68×10^{-6}
800	19	30[a]	119	2.15×10^{-4}
1200	19	9[a]	361	6.56×10^{-4}

568

Table 7. Oxidation of varied graphite material by previous studies[a]

Authors	Sample type/ shape	Oxidant[d]	Δ mass rate (mg cm^{-2} hr^{-1})	Δ mass rate (sec^{-1})	Temp. (°C)	Flow rate (mL min^{-1})	Ref.
Chi & Kim	NGG[b] cylinder	O_2	163–247	-	808	1500	[41]
Fuller	NGG[b] Cylinder	O_2	35	-	750	~500	[30]
Lee	GMM[c] powder	O_2	-	1.50×10^{-5}	750	500	[11]
This study	GMM[c] cylinder	O_2	119	2.15×10^{-4}	800	220	
Gerczak	GMM[c] cylinder	H_2O	-	1.30×10^{-4}	1200	1500	[6]
This study	GMM[c] cylinder	H_2O	79	1.39×10^{-4}	1200	72	

[a]Rate values are reported in units used by authors

[b]Nuclear-grade graphite (NGG)

[c]Graphite matrix material (GMM)

[d]O_2 oxidant testing were conducted at ~21 kPa pO_2 at 800°C and H_2O oxidant testing was conducted at approximately 50 kPa pH_2O at 1200°C

11. Figures

Figure 1

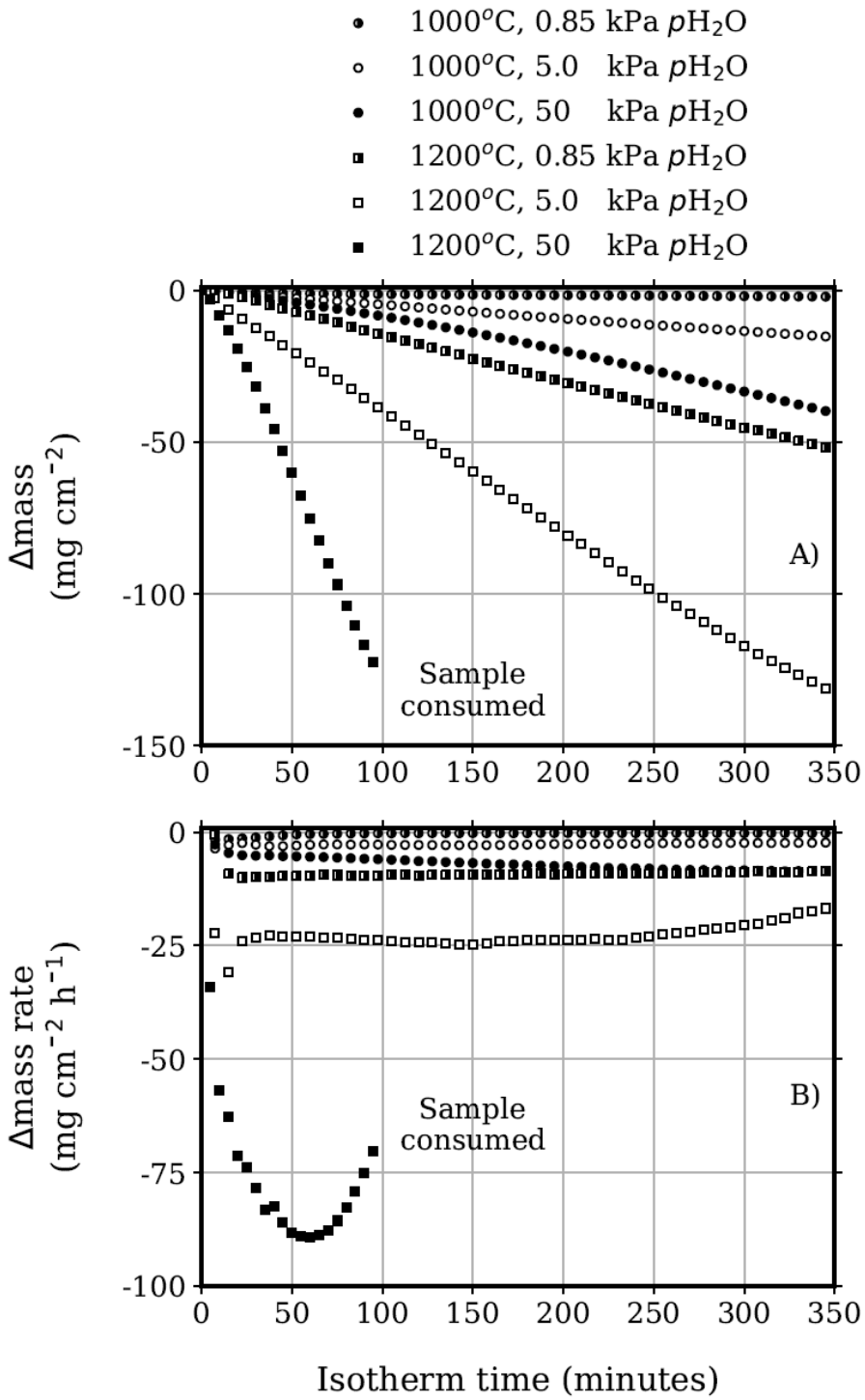

Figure 1. (A) Mass loss and (B) mass rate vs. time in H_2O (g) atmospheres for 1000°C and 1200°C testing conditions; 800°C data not shown. The graphite matrix material sample tested at 1200°C with 50 kPa pH_20 was completely consumed. Both Δmass and Δmass rate are plotted every 12 minutes to5 improve visualization of the data

582 Figure 2

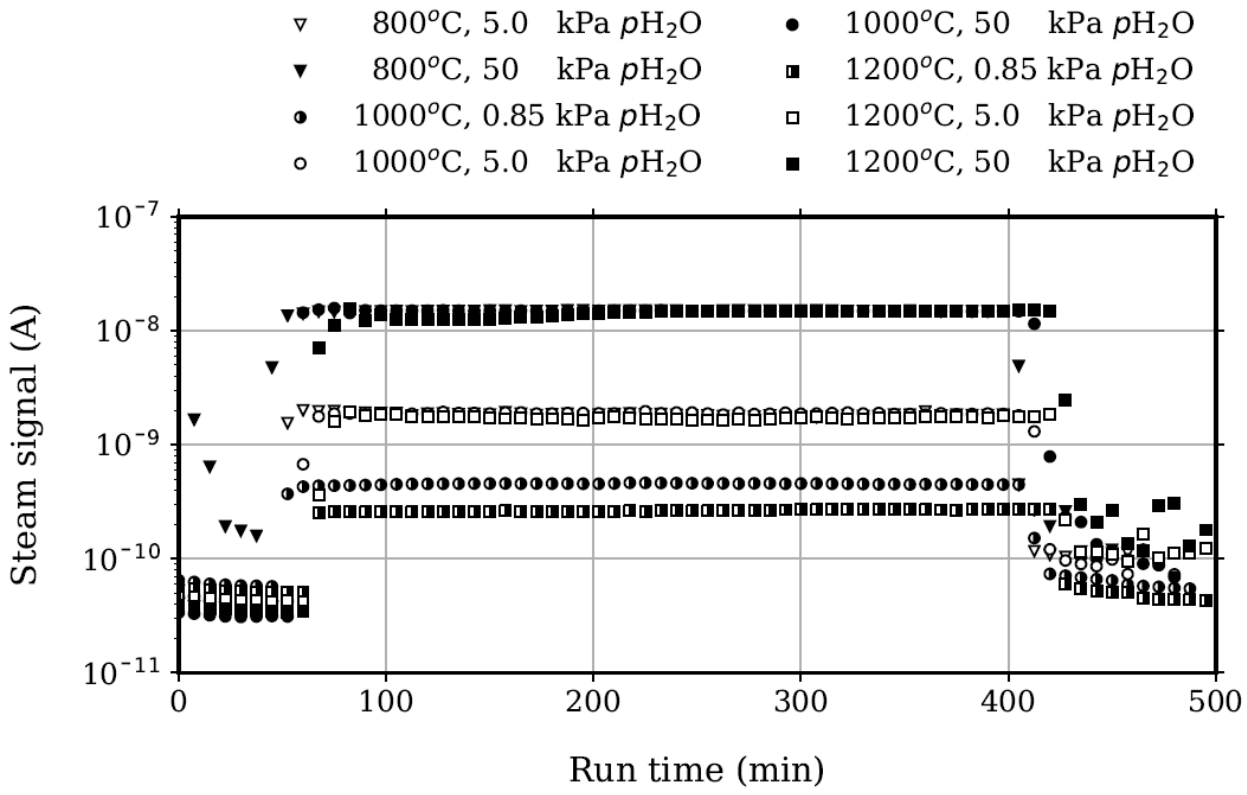

583

584 *Figure 2.* H_2O (g) mass spectrometry signal throughout entire test for each condition. H_2O (g) signal
585 increases dramatically at the start of isotherm. Inconsistent H_2O (g) delivery was most pronounced in 50
586 kPa pH_2O conditions and corresponds to variability in mass loss and oxidation production. Steam mass
587 signal is plotted every 16 mins to improve visualization of the data.

588

589 Figure 3

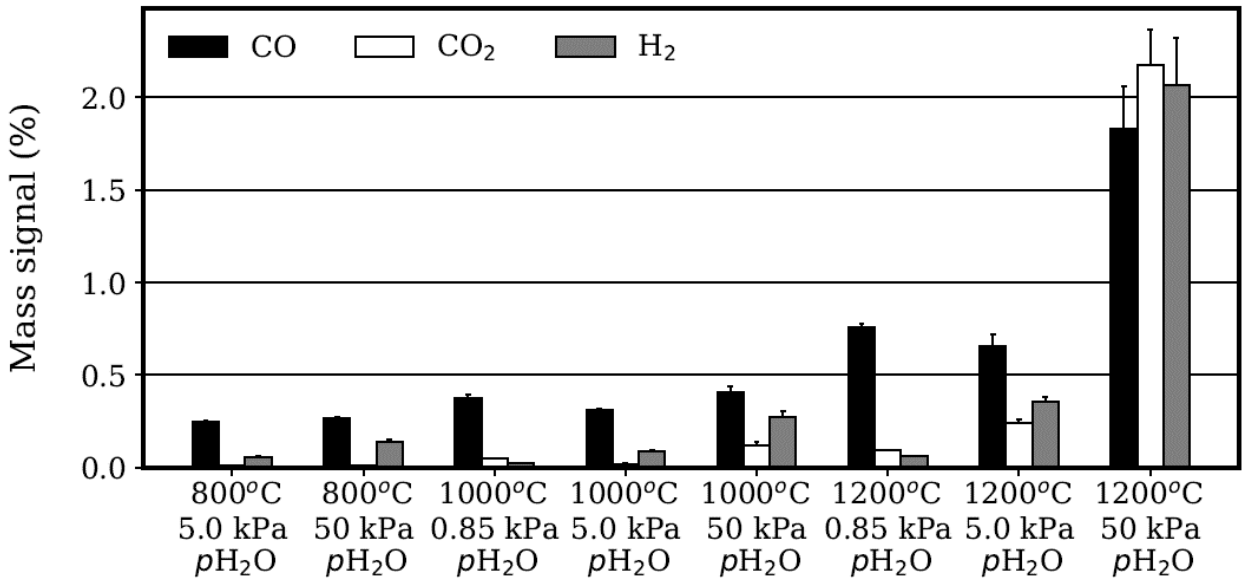

590

591 *Figure 3.* Bar chart demonstrating average mass signal % for six-hour isotherm (and until 20% sample
592 consumption for 50 kPa pH_2O) for CO, CO_2, and H_2 signal. Error bars represent standard deviation.

593 Figure 4

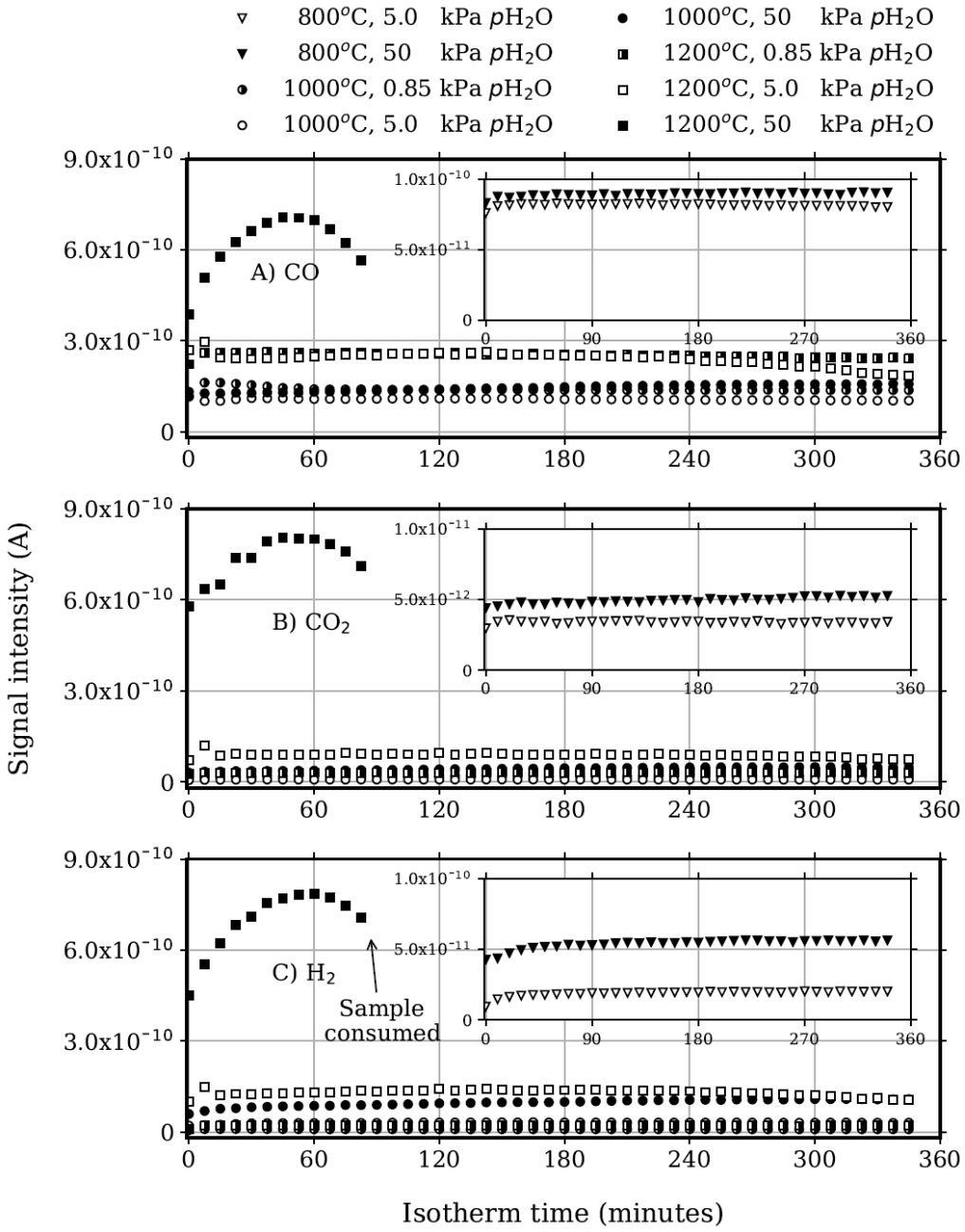

594

595 *Figure 4.* Mass spectrometry signal current for (A) CO, (B) CO_2, and (C) H_2 mass species. Each graph
596 demonstrates mass species for a broad range of temperatures (1000–1200°C) and H_2O (g) atmospheres
597 (0.85–50 kPa pH_2O). Inserts illustrate lower mass spectrometry signals for 800°C testing conditions.
598 Mass signal data is plotted every 12 mins to improve visualization of the data.

599

Figure 5

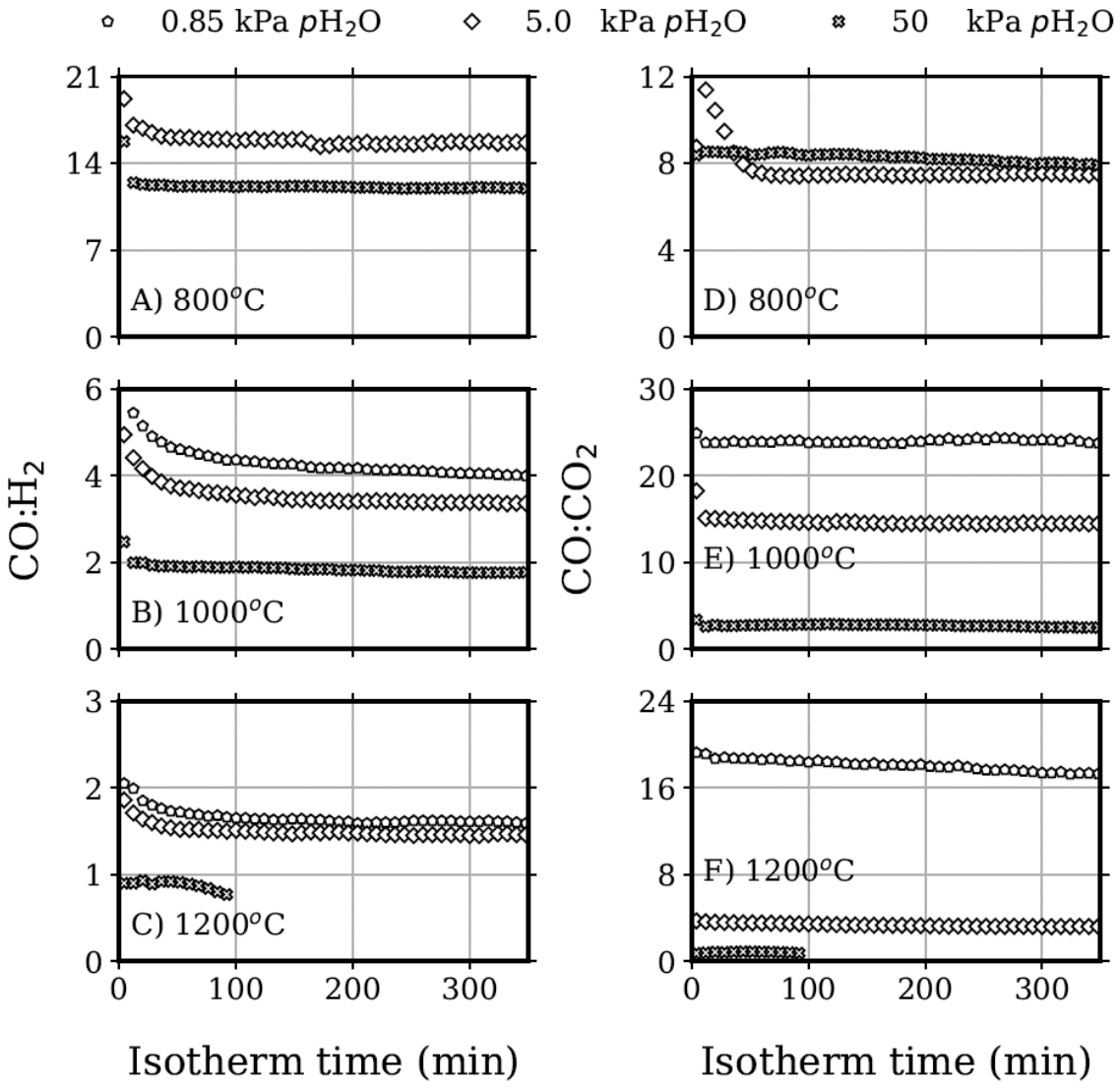

Figure 5. Mass spectrometry ratios for (A) CO:H_2 under 0.85 kPa pH_2O atmosphere, (B) CO:H_2 under 5.0 kPa pH_2O atmospheres, (C) CO:H_2 under 50 kPa pH_2O atmospheres, (D) CO:CO_2 under 0.85 kPa pH_2O atmospheres, (E) CO:CO_2 under 5.0 kPa pH_2O atmospheres, and (F) CO:CO_2 under 50 kPa pH_2O atmospheres. Ratios displayed are 8-minute rolling averages to improve the visualization of the data.

606 Figure 6

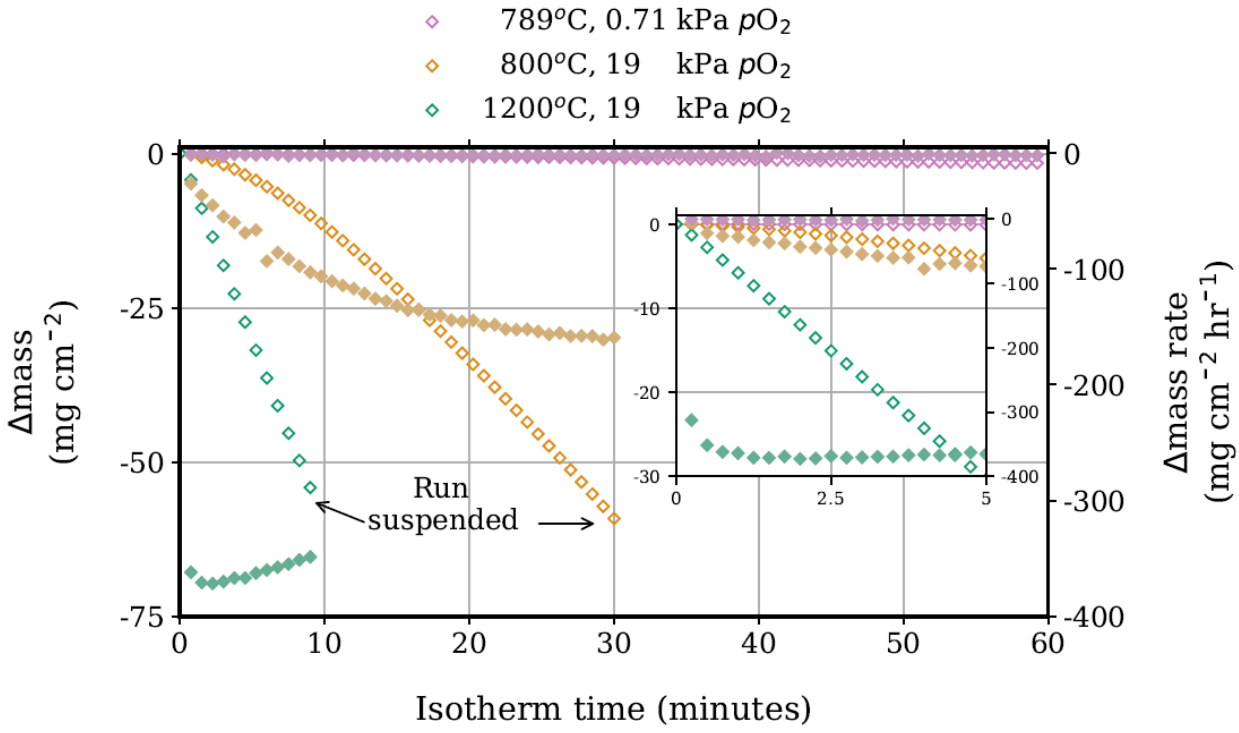

607

608 *Figure 6.* Oxidation of matrix graphite material samples is illustrated at three temperatures and two
609 different O_2 atmospheres. Solid lines demonstrate mass loss (primary y-axis), and diamond symbols
610 demonstrate mass loss rates (secondary y axis). Insert panel examines first 5 minutes of the isotherm to
611 illustrate mass loss during initial oxidation. Tests at 800°C and 1200°C under high pO_2 atmospheres were
612 terminated early to preserve each sample for post-testing scanning electron microscopy analysis.

613 Figure 7

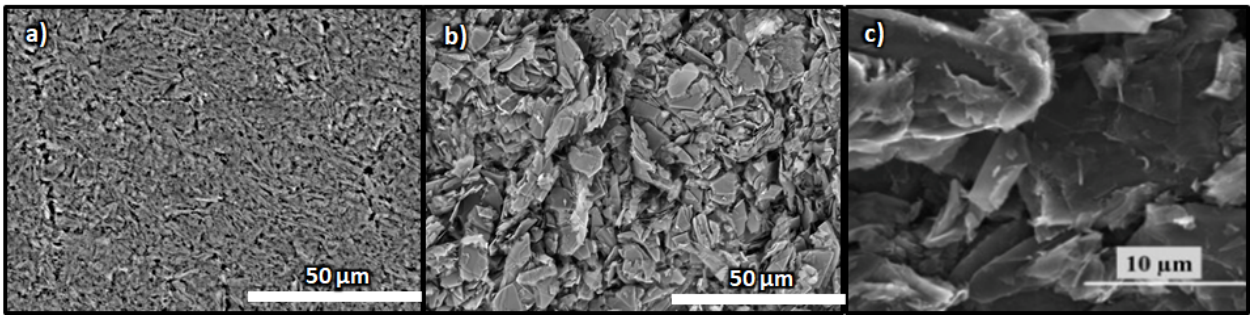

614

615 *Figure 7.* Back scattered electron (BSE) micrographs of characterized microstructure for (a) as received,
616 (b) post 800°C at 19 kPa pO_2, and (c) graphite matrix material post 750°C at 21 kPa pO_2 taken from Lee et
617 al. [11]. Under high pO_2 atmospheres, readily apparent oxidation with clear separation of flakes and the
618 binder can be seen for after pO_2 exposure from this study (b) and Lee et al. [11] (c).

619

620 Figure 8

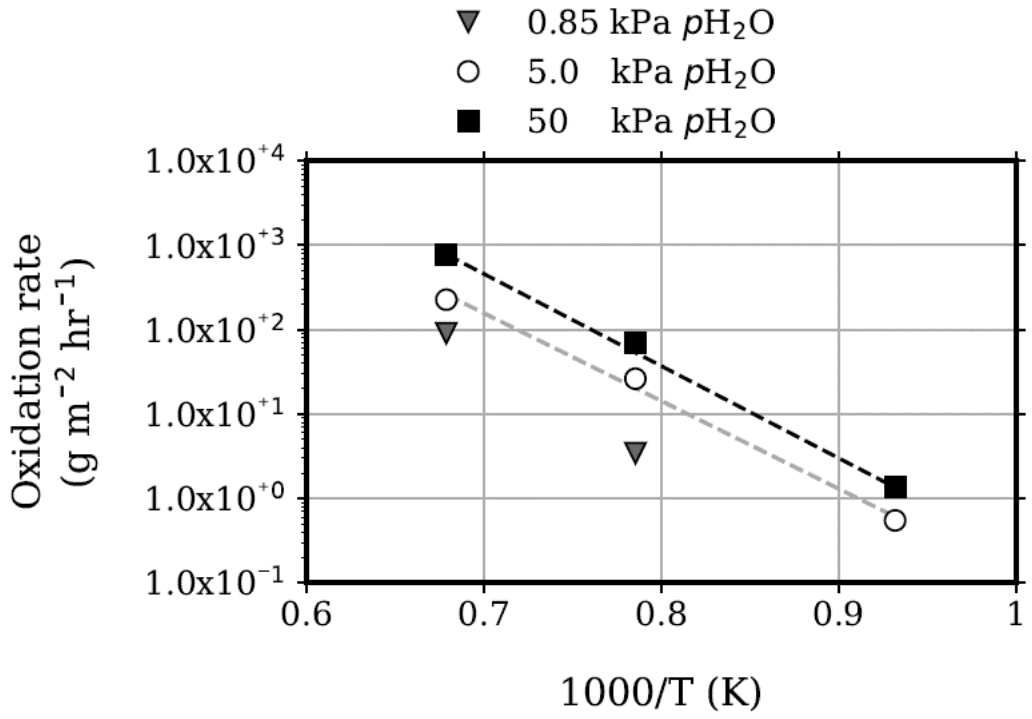

621

622 *Figure 8.* Comparison of Arrhenius data for varied H_2O (g) atmospheres. Data with three H_2O (g)
623 atmospheres are fit with linear regression trend line (r^2 >0.99). Y-axis is log scale.

624 Figure 9

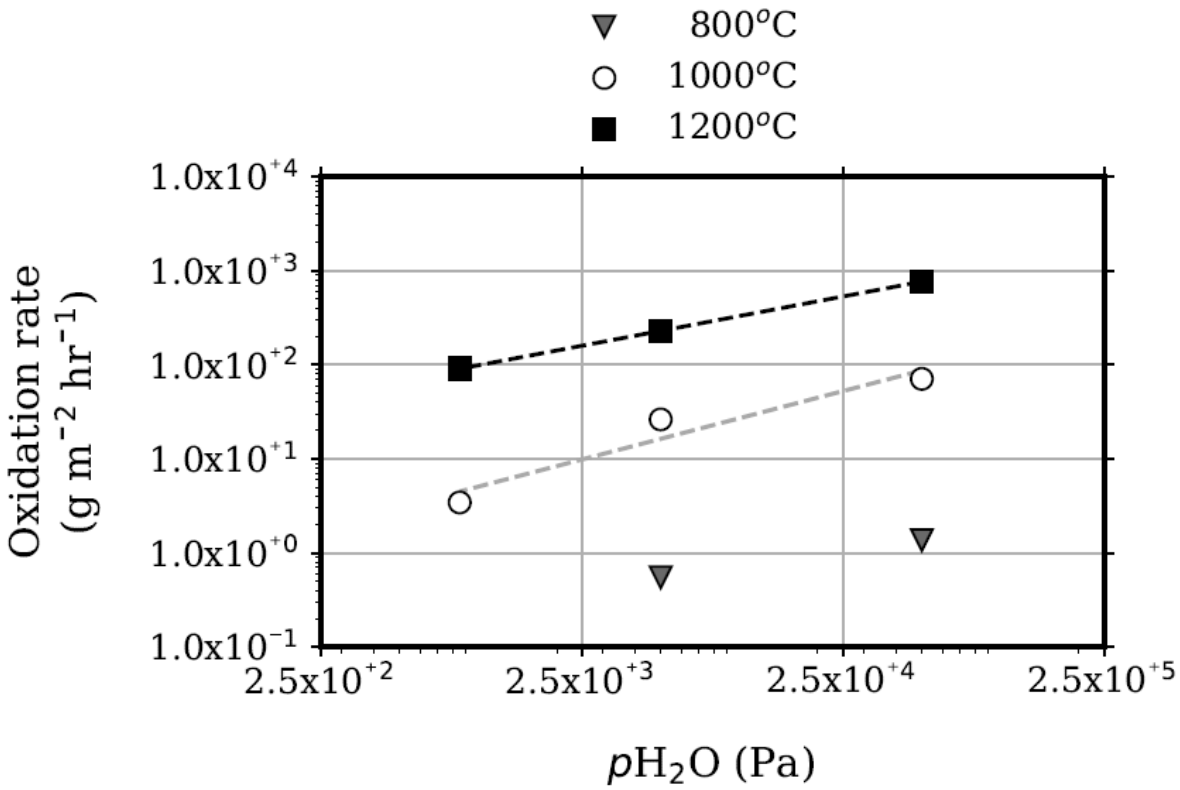

625

626 Figure 9. Measured oxidation rates as a function of pH_2O. Data with three H_2O (g) atmospheres are fit
627 with exponential regression trend line (r^2 >0.99). Both X and Y-axes are log scale.